SUPPLEMENTARY MATERIALS & METHODS

Fluorescence-activated cell sorting of blood biopsies

Peripheral blood mononuclear cells from patients and healthy volunteers were prepared by Ficoll (GE Healthcare, Pittsburgh, Pennsylvania) density-gradient centrifugation. PBMCs were stained with fluorochrome-labeled monoclonal anti-human antibodies to CD19 (clone SJ25C1, eBioscience, San Diego, California), CD8 (clone 3B5, Invitrogen, Carlsbad, California), CD3 (clone UCHT1), CD4 (clone RPA-T4), CD2 (clone TS1/8), CD26 (clone BA5b) (all from Biolegend, San Diego, California) and CD7 (clone M-T701, BD Biosciences, San Jose, California) and sorted on a FACSAria (BD Biosciences, San Jose, California) into tumor (atypical CD4+ T cells characterized by the loss of CD7 and/or CD26) and non-tumor (CD19+ CD3-) cell populations. Tumor burden was assessed by number of atypical T cells observed per ml of blood. Non-malignant memory and naïve CD4+ T cells were FACS-sorted from peripheral blood of healthy volunteers. Memory and naïve CD4 T cells were gated according to positive staining for CD3, CD4, and CD45RO (clone UCHL1, Biolegend, San Diego, California) and CD45RA (clone HI100, ebioscience, San Jose, California) respectively.

DNA isolation

Genomic DNA was isolated from sorted SS tumor cells using the DNeasy Blood and Tissue kit (Qiagen, Venlo, Netherlands), per the manufacture's instructions. Matched DNA was isolated from peripheral blood B cells for WES analysis.

Whole exome library preparation and sequencing

250 ng of DNA from each sample were sheared to an average of 150 bp in a Covaris instrument (Woburn, Massachusetts) for 360 seconds (Duty cycle - 10%; intensity - 5; cycles/Burst - 200). Barcoded libraries were prepared using the Kapa Low-Throughput Library Preparation Kit Standard (Kapa Biosystems, Wilmington, Massachusetts), amplified using the KAPA HiFi Library Amplification kit (Kapa Biosystems) (8 cycles) and quantified using Qubit Fluorimetric Quantitation (Invitrogen, Carlsbad, California) and Agilent Bioanalyzer (Santa Clara, California). An equimolar pool of the 4 barcoded libraries (300 ng each) were used as input to capture the exome using one reaction tube of the Nimblegen SeqCap EZ Human Exome Library v3.0 (Roche, cat # 06465684001), according to the manufacturer's protocol. The pooled capture library was quantified by Qubit (Invitrogen, Carlsbad, California) and Bioanalyzer (Agilent, Santa Clara, California) and sequenced on an Illumina HiSeq 2500 (San Diego, California) using a paired end, 100 nucleotide in length run mode, to achieve an average of 100X coverage. Sequences will be deposited in the Sequencing Read Archive upon publication.

DNA sequencing analysis

Reads were aligned to the hg19 genome build (GRCh37) using the Burrows-Wheeler Aligner (BWA). Further indel realignment, base-quality score recalibration and duplicate-read removal were performed using the Genome Analysis Toolkit (GATK) v2.4-9. Somatic Sniper v1.0.0 and GATK Somatic Indel Detector were used to generate single-nucleotide variation (SNV) and indel calls, respectively, using standard, default parameters. Sequences from tumor cells were compared to those from B cells isolated from the same patient to identify somatic mutations. This method excludes possible mutations that may be originating from lymphoid progenitors;

future studies will compare tumor DNA to other hematopoietic lineages and cheek swabs. MuTect was used to confirm SNV calls with the conditions described previously (Banerji et al. 2012). Baseline filters (depth of 3× coverage in both tumor and normal specimens, >97% normal allelic fraction, >10% tumor allelic fraction) were chosen. We excluded germline variants found in the 1000 Genomes Project, ESP5400 (National Heart, Lung, and Blood Institute (NHLBI) GO Exome Sequencing Project), and dbSNP132. Further filtering was based on mapping quality score, average read length and strand bias, as previously described(Larson et al. 2012). Resulting mutations were annotated based on RefSeq (Release 55) using Annovar. All candidates were manually inspected via Integrative Genomics Viewer (IGV) v2.1.

The impacts of the mutations were measured by Polyphen-2 (Adzhubei et al. 2010), a probabilistic classifier based on machine learning that is optimized for high-throughput annotation of amino-acid substitutions. Polyphen-2 predicts the functional significance of an SNV by location in a protein domain and cross-species sequence conservation. Identified SNVs were considered to be likely deleterious by have a coverage of > 14 reads and a PolyPhen-2 score of ≥ 0.5 (out of 1). Gene function and pathway association was inferred from Ingenuity Pathway Analysis (Qiagen, Redwood City, California).

To identify regions with large-scale copy-number variation, we used the software Control-FREEC (Wang et al. 2010) which uses information on read depth to call copy number variants. Control-FREEC does not require sequences from a reference sample, and controls for variation in GC content, a major source of variability in read depth. We ran Ctrl-FREEC 6.4 in sliding windows of 50 kb on the realigned tumor sequences (in a pileup format) matched with the

corresponding normal sequences. The copy number analysis was restricted to the exonic regions defined by the capture file.

Digital droplet PCR (ddPCR)

CNV of *MYC, TP53,* and *PTEN* were validated by digital droplet PCR (Biorad, Hercules, California). 3 ng of genomic DNA from each sample was assayed by ddPCR according to manufacturer's instructions. Samples were run in duplicate. Primers and probes used are as follows: *MYC* (UniqueAssayID: dHsaCP2500322)*, TP53* (UniqueAssayID: dHsaCP1000586)*,* and *PTEN* (UniqueAssayID: dHsaCP2500323) were provided by Biorad in FAM fluorophore. Custom primers and probe to *STAT3* are as follows: FOR: 5'-CCAGCAAAGAATCACATGCC-3', REV: 5'-CTTGCAGGAAGCGGCTATAC-3', probe: 5'-TCTCCTGGGAGAGATTGA CCAGCA-3' in FAM fluorophore. Reference probes for *RPP30* (UniqueAssayID: dHsaCP1000485) *EIF2C1* (UniqueAssay ID: dHsaCP1000002) were also provided by Biorad in HEX fluorophore. For patient samples R14, R10, and R17, WES CNV analysis determined a single copy number loss in reference gene *RPP30;* during computation analysis of CNV by ddPCR we therefore adjusted the reference gene value.

RNA isolation, library preparation, and sequencing

RNA was isolated from human samples using RNeasy Kit (Qiagen). 100 ng of total RNA from each sample was used to prepare an RNA sequencing library using the TruSeq Stranded Total RNA with Ribo-Zero Gold Library Preparation Kit (Illumina, San Diego, California), per manufacturers instructions. The pooled library was quantified by Bioanalyzer (Agilent, Santa Clara, California) and checked for quality by Tape Station (Agilent, Santa Clara,

California). For murine samples RNA was isolated using the Pico Pure RNA isolation Kit (Applied Biosystems). The Library was prepared with SMART-Seq v4 Ultra Low Input RNA kit (Clontech Laboratories). The library was sequenced on an Illumina HiSeq 2500 (San Diego, California) using a paired end, 50 nucleotide in length run mode using v4 chemistry. Sequences will be deposited in the Sequencing Read Archive upon publication.

RNA sequencing analysis

Sequencing results were demultiplexed and converted to FASTQ format using Illumina Bcl2FastQ software. Paired-end reads were aligned to the human genome (build hg19/GRCh37) using the splice-aware STAR aligner (Dobin et al. 2012). PCR duplicates were removed using the Picard toolkit. HTSeq package was utilized to generate counts for each gene based on how many aligned reads overlap its exons (Anders et al. 2015). These counts were then used to test for differential expression using negative binomial generalized linear models implemented by the DESeq2 R package (Love et al. 2014). Ingenuity Pathway Analysis (Qiagen, Redwood City, California) and the Gene Ontology Consortium (Ashburner et al. 2000) were used to infer gene pathway association.

Silhouette Plot

Silhouette analysis was performed with as previously described (Rousseeuw 1987).

Gene Set Enrichment Analysis

GSEA (Subramanian et al. 2005) analysis was performed using an online tool provided by the MIT Broad Institute at http://www.broadinstitute.org/gsea/index.jsp.

Cell Culture Experiments

SeZ4 (SS cell line) and Myla2059 (MF cell line) were generously provided by Dr. Kaltoft. SeZ4 cells are cultured in RPMI 1640 medium with 1% L glutamine, 1% pen/step, 1000units/ml of rh IL-2 (BD Biosciences, San Jose, California), and 10% human serum. Myla 2059 cells are cultured in RPMI 1640 medium with 1% L glutamine, 1% pen/step, and 10% fetal bovine serum. Cells incubated at 37°C, 5% CO2. For cell number and cell death assay, cells were treated with STAT3 inhibitor STA-21 (Enzo Life Sciences, Farmingdale, New York) at 80μM concentration or equivalent volume of DMSO for control. Total cell number and number of dead cells were enumerated using a Beckman-Coulter Vi-Cell XR machine. These two cell lines are patient derived and displaying constitutive Stat3 activation, which is inhibited by STA-21(Krejsgaard et al. 2013; Fredholm et al. 2016; Vieyra-Garcia et al. 2016)

Generation of STAT3C^{stopfl} mouse and colony maintenance

C57BL/6 STAT3C$^{stopfl/+}$ mice were generated previously (Mesaros et al. 2008). Mice are housed in specific pathogen free conditions in the Skirball barrier animal facility at NYU School of Medicine and treated according to the guidelines of the Institutional Animal Care and Usage Committee. Control mice were mixed genotype but were generally mice that were heterozygous for the floxed stop cassette and that lacked CD4Cre. Controls were age-matched, littermates, and cage-mates when possible. Mice of both sexes were analyzed at pre-determined ages (between 4-16 months), or upon disease phenotype progression. Germ free STAT3C$^{stopfl/+}$ CD4Cre were generated via aseptic hysterectomy and cross-fostering with germ free dams at Taconic Biosciences and transferred to NYU germ free facility. Absence of bacteria and fungi are routinely confirmed via culture-based, 16S and 18S methods. Conventionalized mice were born

into germ free conditions and then housed with SPF animals shortly after weaning. Rag2KO (Shinkai et al. 1992) and OTII (Barnden et al. 1998) mice were purchased from Jackson laboratories and crossed to STAT3C$^{stopfl/+}$ mice.

Histopathology

Murine skin was shaved and removed from mouse. Skin was placed in tissue cassette and fixed in 10% formalin for 24 to 48 hours. Skin was washed in PBS and then stored in 70% ethanol until paraffin embedding. Tissues were sectioned in 5-um slices and stained with H&E, or with antibodies against CD3 (clone 2GV6, Roche Ventana, Tuscan, Arizona) or Ki-67 (clone SP6, Thermo Scientific). Immunohistochemistry was performed on a Ventana Medical Systems Discovery XT platform using Ventana's reagents and detection kits. Slides were counterstained with hematoxylin. CD4 (clone EPR19514, Abcam) staining was performed by HistoWiz Inc. The images were scanned with Leica SCN400 slide scanner. The software used was Leica Slidepath Digital Image Hub. Blood smears were stained with Wright-Giemsa stain. Images were obtained with an Olympus BX53 microscope. 1000x. Immunofluorescence staining was performed as described (Vaeth et al. 2016) Antigen retrieval was carried out using 10 mM citric acid (pH 6.0). Primary antibodies rabbit anti-CD3 (1:1000 dilution; Dako A0452) and rat anti-CD8a (1:100 dilution; clone 4SM16 eBioscience) were incubated at 4°C overnight. After washing anti-CD8a antibody was amplified using biotinylated goat anti-rat IgG (Molecular Probes). Final detection was performed using donkey anti-rabbit Alexa Fluor 488 (1:800 dilution, Life Technologies) and goat anti-rabbit IgG Alexa Fluor 546 (both 1:800 dilution, Life Technologies). Samples were embedded using Fluoromount-G with DAPI (eBioscience) and

images were taken using a Leica TCS SP5 II confocal microscope. Data was processed using the LCS software package (Leica) and ImageJ (NIH).

Flow cytometric analysis and sorting of murine samples

Single cell suspensions of murine ear skin were obtained for analysis. Skin was minced, digested in 2.5 mg/ml of Type I-A collagenase (Sigma-Aldrich, St. Louis, Missouri) and 62 units/ml of DNAse (Worthington Biochemical, Lakewood, New Jersey) diluted in HBSS (Invitrogen, Carlsbad, California) and incubated at 37C for 1.5 hours. Skin was then digested in 0.25mg/ml of Liberase TL (Roche, Basal, Switzerland) and 0.5 mg/ml DNase (Sigma, St. Louis, Missouri) diluted in RPMI and incubated for 1.5 hours at 37°C. Cells were filtered through a 70-uM cell strainer. Lymph nodes and thymi were mechanically disrupted and filtered through a 70-uM cell strainer. Cells stained for intracellular cytokines were stimulated and treated with a PMA, ionomycin, brefeldin A, and monensin mix (eBioscience, San Jose, California) and incubated for 4 hours at 37°C. Cells were surface stained, fixed with 2% PFA and permeabilized with 0.5% saponin, and intracellulary stained for cytokine expression. The following fluorochrome conjugated antibodies were used: IL-17A (clone TC11-18H10.1, Biolegend), CD8 b.2 (clone 53-5.8, Biolegend), CD3 (clone 145-2C11), CD4 (clone RM4-5), CD44 (clone IM7), CD62L (clone MEL-14), IFNγ (clone XMG1.2), IL-22 (clone 1H8PWSR), and IL-4 (clone 11B11) (all from eBioscience). Ki-67 (clone B56, BD Biosciences) and RORγt (clone Q31-378, BD Biosciences) staining occurred following permeabilization with fix/perm buffer (eBioscience). Samples were run on a BD Fortessa and analyzed using FlowJo software. For data analysis, cells were gated on the lymphocyte population and then doublet cells were excluded. Cells were gated on CD3+ CD4+ T cells. For RNA sequencing experiments cells were gated on CD3+CD4+ and sorted

using SY3200 (Sony) cell sorter. Data from mice aged 6-16 months old is shown, unless otherwise noted.

Adaptive Biotechnologies

Amplification and sequencing of TCRB CDR3 was performed using the immunoSEQ Platform (Adaptive Biotechnologies®, Seattle, WA). The immunoSEQ Platform combines multiplex PCR with high throughput sequencing and a sophisticated bioinformatics pipeline for TCRB CDR3 analysis (Robins et al. 2009; Carlson et al. 2013).

Animal behavior monitoring

Mice were housed from 2 to 14 months of age in Vium's AAALAC-accredited Digital Vivarium™ in accordance with the NIH Guide for the Care and Use of Laboratory Animals and were approved by Vium's Institutional Animal Care and Use Committee. The number of mice found to be scratching was assessed by observers blind to genotype. 5 mice of each genotype were monitored and scratching behavior was assessed during one 10 minute segment of video recorded during the dark cycle in the vivarium per day for 5 months by an independent contractor.

Statistics

A minimum of 3 independent experiments was performed unless otherwise stated. For Figure 2, statistical significance was assessed using 2 way ANOVA with Sidak's multiple comparison post-test. Statistical significance was assessed using the nonparametic Mann-Whitney U test, two-tailed p value for the flow cytometry data. For Figure 3d, a Wilcoxon Signed Rank Test was performed. Variance between groups being compared was observed to be similar. For Figure 5c

a 2 way ANOVA with Bonferroni post-test was performed. Significance values were as follows ns ($p > 0.05$), * ($p \leq 0.05$), ** ($p \leq 0.01$), *** ($p \leq 0.001$) **** ($p \leq 0.0001$). Data was analyzed with Prism (GraphPad, La Jolla, California)

REFERENCES

Adzhubei IA, Schmidt S, Peshkin L, Ramensky VE, Gerasimova A, Bork P, et al. A method and server for predicting damaging missense mutations. Nat Methods 2010 Apr 1;7(4):248–9.

Anders S, Pyl PT, Huber W. HTSeq--a Python framework to work with high-throughput sequencing data. Bioinformatics 2015 Jan 8;31(2):166–9.

Ashburner M, Ball CA, Blake JA, Botstein D, Butler H, Cherry JM, et al. Gene Ontology: tool for the unification of biology. Nat Genet 2000 May;25(1):25–9.

Banerji S, Cibulskis K, Rangel-Escareno C, Brown KK, Carter SL, Frederick AM, et al. Sequence analysis of mutations and translocations across breast cancer subtypes. Nature 2012 Jun 11;486(7403):405–9.

Barnden MJ, Allison J, Heath WR. Defective TCR expression in transgenic mice constructed using cDNA-based α-and β-chain genes under the control of heterologous regulatory elements. Immunology and cell biology1998;76(1):34–40.

Carlson CS, Emerson RO, Sherwood AM, Desmarais C, Chung M-W, Parsons JM, et al. Using synthetic templates to design an unbiased multiplex PCR assay. Nature Communications 2013 Oct 16;4:1–9.

Dobin A, Davis CA, Schlesinger F, Drenkow J, Zaleski C, Jha S, et al. STAR: ultrafast universal RNA-seq aligner. Bioinformatics 2012 Dec 20;29(1):15–21.

Fredholm S, Litvinov IV, Mongan NP, Schiele S, Willerslev-Olsen A, Petersen DL, et al. The Expression of IL-21 Is Promoted by MEKK4 in Malignant T Cells and Associated with Increased Progression Risk in Cutaneous T-Cell Lymphoma. J Invest Dermatol 2016 Apr;136(4):866–9.

Krejsgaard T, Litvinov IV, Wang Y, Xia L, Willerslev-Olsen A, Koralov SB, et al. Elucidating the role of interleukin-17F in cutaneous T-cell lymphoma. Blood 2013 Aug 8;122(6):943–50.

Larson DE, Harris CC, Chen K, Koboldt DC, Abbott TE, Dooling DJ, et al. SomaticSniper: identification of somatic point mutations in whole genome sequencing data. Bioinformatics 2012 Jan 30;28(3):311–7.

Love MI, Huber W, Anders S. Moderated estimation of fold change and dispersion for RNA-seq data with DESeq2. Genome Biol 2014;15(12):550–21.

Mesaros A, Koralov SB, Rother E, Wunderlich FT, Ernst MB, Barsh GS, et al. Activation of Stat3 Signaling in AgRP Neurons Promotes Locomotor Activity. Cell Metabolism 2008 Mar;7(3):236–48.

Robins HS, Campregher PV, Srivastava SK, Wacher A, Turtle CJ, Kahsai O, et al. Comprehensive assessment of T-cell receptor beta-chain diversity in alphabeta T cells. Blood 2009 Nov 5;114(19):4099–107.

Rousseeuw PJ. Silhouettes: a graphical aid to the interpretation and validation of cluster analysis. Journal of computational and applied mathematics 1987;20:53–65.

Shinkai Y, Rathbun G, Lam KP, Oltz EM, Stewart V, Mendelsohn M, et al. RAG-2-deficient mice lack mature lymphocytes owing to inability to initiate V(D)J rearrangement. Cell 1992 Mar 6;68(5):855–67.

Subramanian A, Tamayo P, Mootha VK, Mukherjee S, Ebert BL, Gillette MA, et al. Gene set enrichment analysis: a knowledge-based approach for interpreting genome-wide expression profiles. Proc Natl Acad Sci USA 2005 Oct 25;102(43):15545–50.

Vaeth M, Eckstein M, Shaw PJ, Kozhaya L, Yang J, Berberich-Siebelt F, et al. Store-Operated Ca2+ Entry in Follicular T Cells Controls Humoral Immune Responses and Autoimmunity. Immunity 2016 Jun 21;44(6):1350–64.

Vieyra-Garcia PA, Wei T, Naym DG, Fredholm S, Fink-Puches R, Cerroni L, et al. STAT3/5-Dependent IL9 Overexpression Contributes to Neoplastic Cell Survival in Mycosis Fungoides. Clin Cancer Res 2016 Jul 1;22(13):3328–39.

Wang K, Li M, Hakonarson H. ANNOVAR: functional annotation of genetic variants from high-throughput sequencing data. Nucl Acids Res 2010 Sep 10;38(16):e164–4.

Supplementary Figure 1.

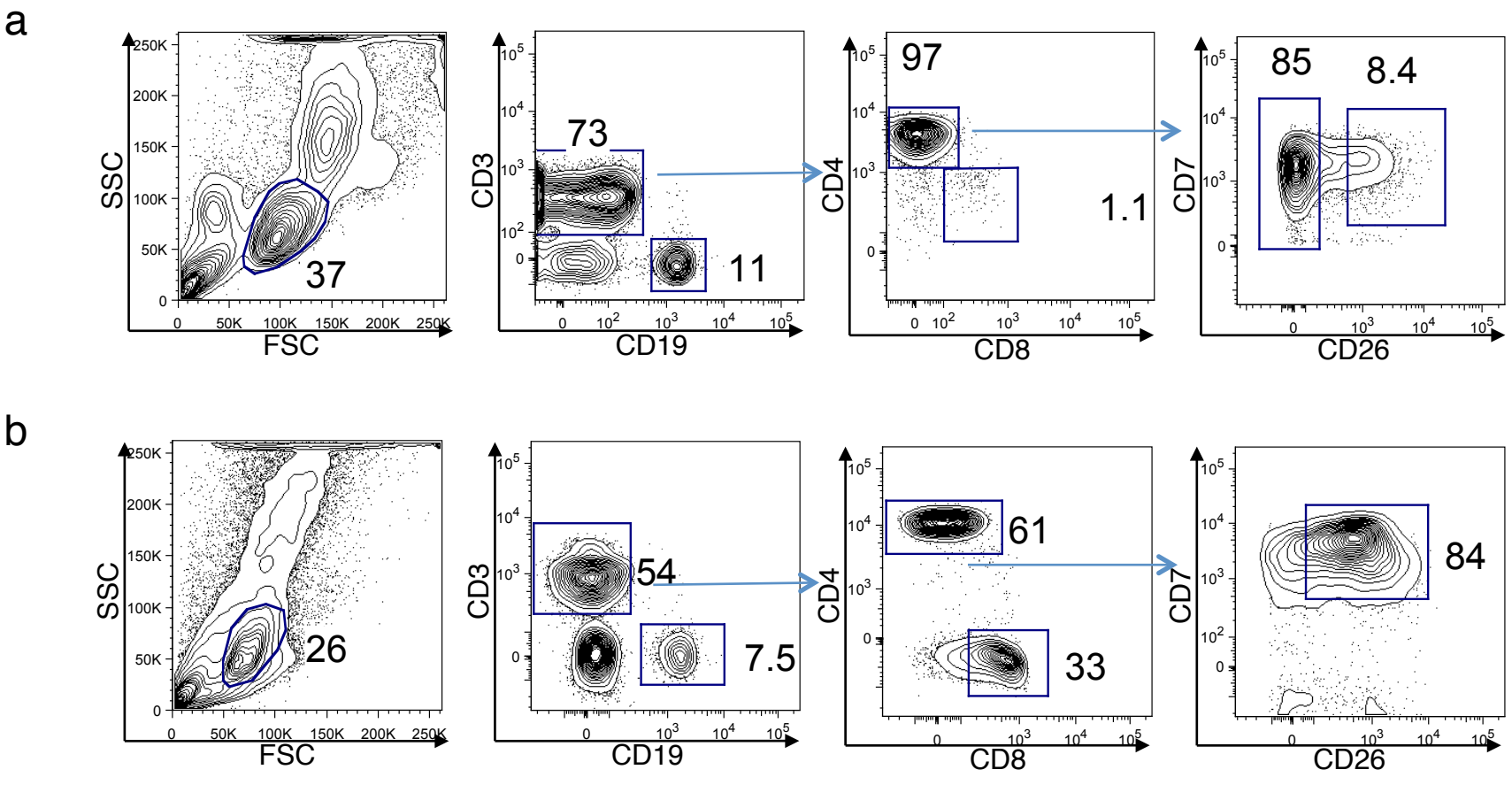

Figure S1. Representative surface marker analysis of SS leukemic cells
(a) Gating strategy for flow cytometric analysis and sorting of SS patient atypical T cells (CD7- and/or CD26-) and normal B cells (CD19+ CD3-) from purified peripheral blood mononuclear cells (PBMCs). (b) FACS analysis and sorting strategy of T lymphocytes from a healthy volunteer.

Supplementary Figure 2.

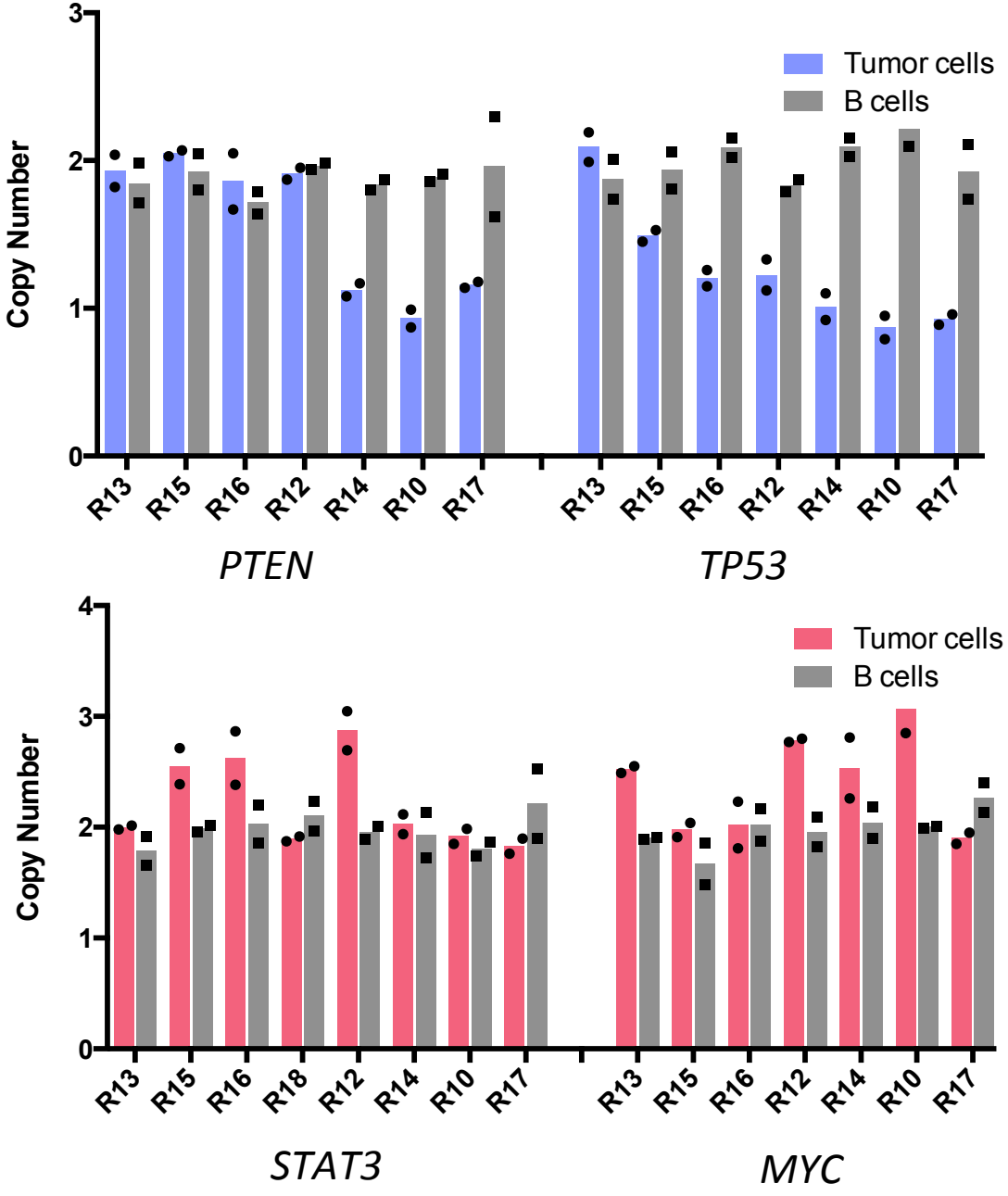

Figure S2. Copy number losses and gains validated via digital droplet PCR
Validation of gene copy number losses (top) and gains (bottom) observed in WES by digital droplet PCR. Genes of interest were normalized to reference gene RPP30 or EIF2C1. Experiment was performed with two technical replicates.

Supplementary Figure 3.

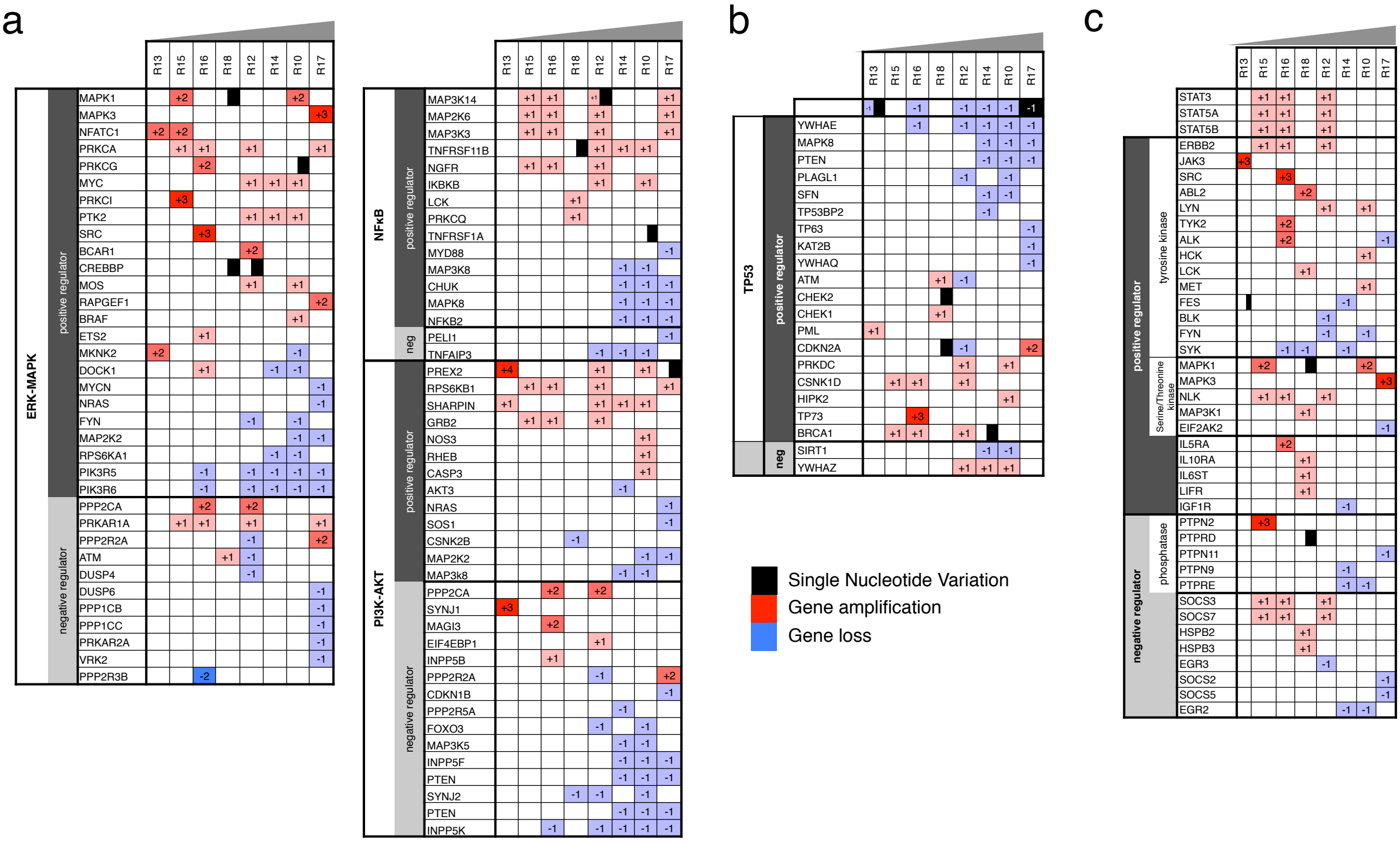

Figure S3. Heterogeneous sets of genetic perturbations converge on several distinct pathways in SS.
(a-c) Tables depicting SNV and CNVs in pathways commonly dysregulated in cancer. Each column denotes an individual patient, increasing in tumor burden from left to right. Numbers in red-shaded cells indicate the copy number gained. Numbers in blue-shaded cells indicate the copy number lost. Cells filled black indicate likely deleterious SNV. Genes were selected based on their known associations with cancer-relevant pathways and appreciable expression levels in human CD4+ T cells. (a) SNV and CNVs of genes in pathways known to promote cancer progression (ERK-MAPK, NFκB, PI3K-AKT), separated by positive and negative regulators of signaling. Genes of the PTEN pathway are incorporated as positive and negative regulators of the PI3K-AKT pathway. Genes encoding proteins involved in multiple pathways were only listed once. (b) Mutations identified in the p53 tumor suppressor pathway. Patient R13 was found to have three copies of *TP53* containing a deletion, and one normal copy. Patient R17 had loss of one copy of *TP53* with a SNV in the remaining copy. (c) Mutations identified in the STAT3/STAT5 signaling pathway. Tyrosine and serine/threonine kinases known to phosphorylate STAT3/STAT5 with observed CNV and SNV are noted, as are phosphatases known to dephosphorylate STAT3/STAT5.

Supplementary Figure 4.

Heatmap of gene expression level of CTCL “signature” genes within independent cohort of patient and control biospecimens

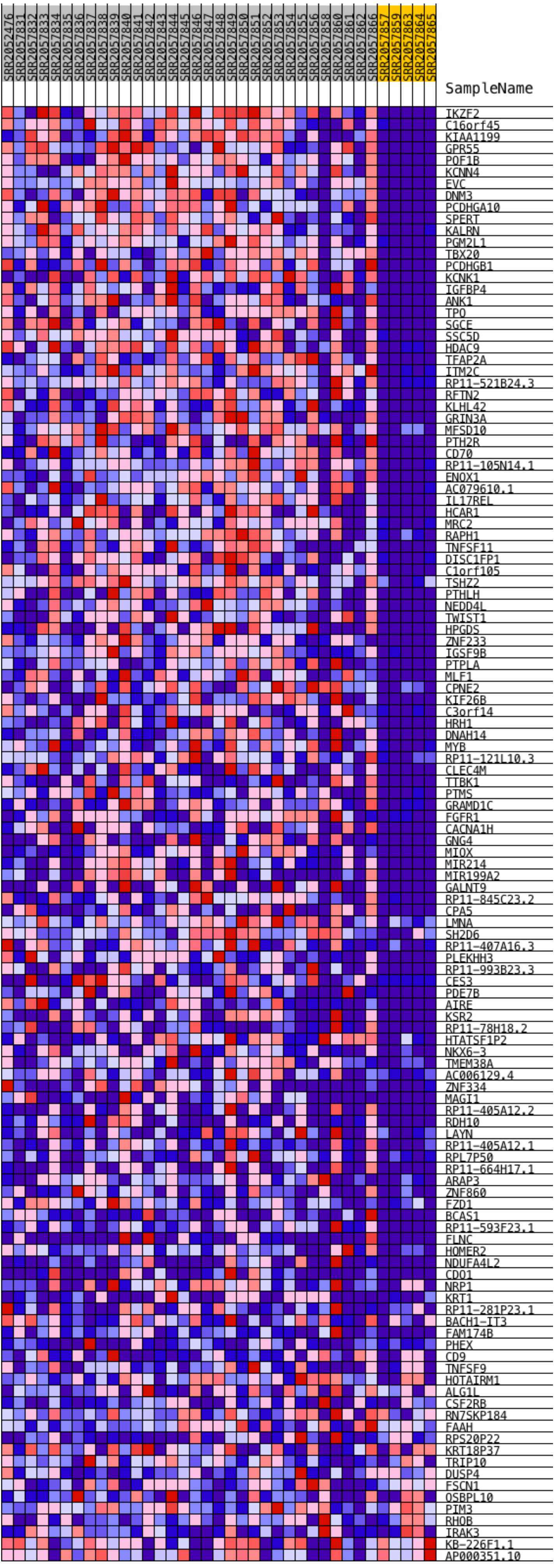

Figure S4. Heatmap of gene expression level of CTCL “signature” genes within independent cohort of patient and control biospecimens

Heatmap of gene expression in the previously published RNA sequencing of CTCL patients and controls highlighting the utility of the CTCL gene expression signature that we identified. CTCL patient samples are in grey and Healthy Volunteer samples are in yellow. Shades of red denote increased gene expression and blue reveals decreased expression.

Supplementary Figure 5.

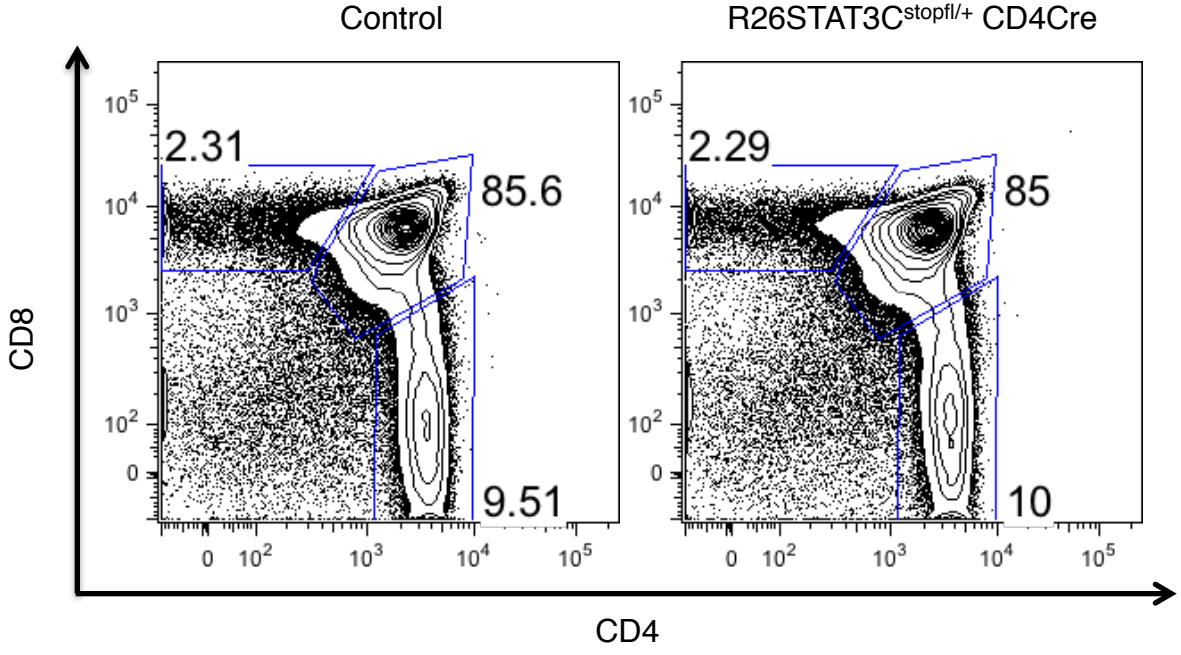

Figure S5. T cells develop normally in the thymus with no differences in T cell percentages in thymus of young mice. Representative flow cytometry plot of CD4 and CD8 thymic T cell populations in 18 day old *R26STAT3C$^{stopfl/+}$ CD4Cre* mouse and littermate control. Events are gated on single lymphocytes. Data is representative of 3 independent experiments.

Supplementary Figure 6.

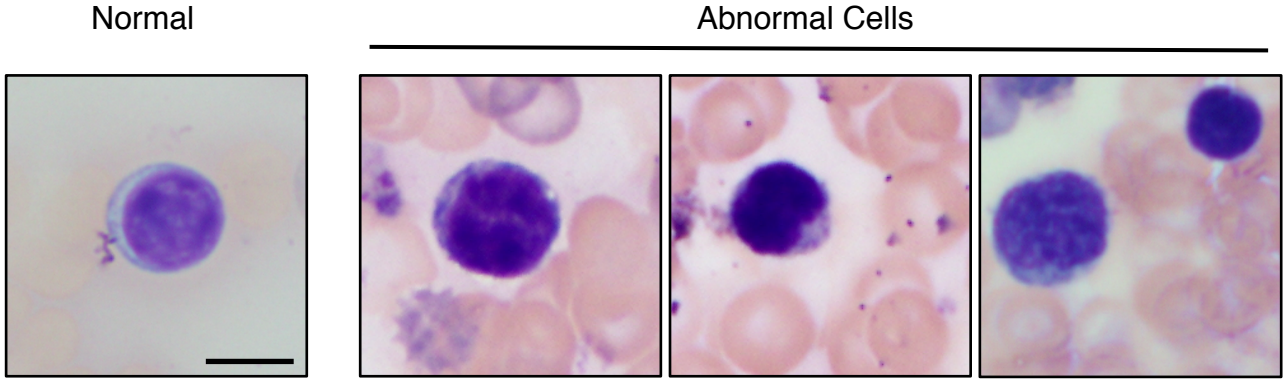

Figure S6. Lymphocytes with atypical nuclei occasionally present in the blood of *R26STAT3C$^{stopfl/+}$ CD4Cre* mice.
Blood smears from 11-month-old *R26STAT3C$^{stopfl/+}$ CD4Cre* mice visualized with Wright-Giemsa stain. Scale bar = 5 μm.

Supplementary Figure 7.

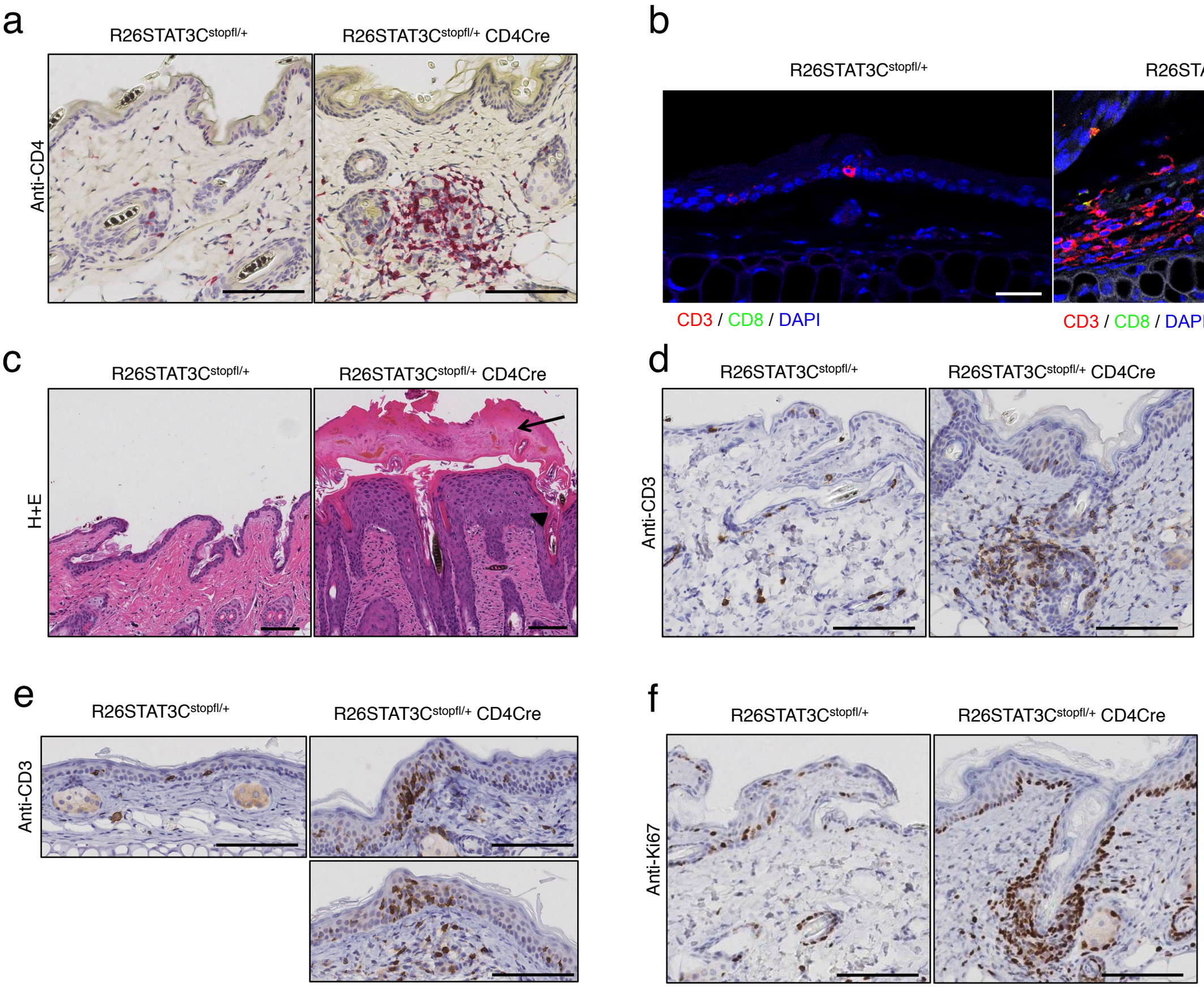

Figure S7. The skin of *R26STAT3C$^{stopfl/+}$ CD4Cre* mice show thickened epidermis and hyperkeratosis accompanied by increased infiltration and proliferation of T Cells compared to controls.
Skin sections from control (left) and *R26STAT3C$^{stopfl/+}$ CD4Cre* (right) mice, aged 10-11 months old. Scale bar = 100 μm unless otherwise stated.(a) Anti-CD4 staining highlights a characteristic cluster of CD4+ T cells in the flank skin of an *R26STAT3C$^{stopfl/+}$ CD4Cre* mouse (b) anti-CD3 (red), anti-CD8 (green), and Dapi (blue) staining in ear skin. CD8+CD3+ T cells stain yellow. Scale bar = 20 μm. (c) H&E. arrowhead points to acanthosis, while the arrow highlights an area of hyperkeratosis. (d) Anti-CD3 staining highlights a characteristic cluster of T cells in the flank skin of an *R26STAT3C$^{stopfl/+}$ CD4Cre* mouse, reminiscent of Pautrier microabscess. (e) Anti-CD3 staining highlights clusters of T cells in the epidermis of ear skin of an *R26STAT3C$^{stopfl/+}$ CD4Cre* mouse (f) Anti-Ki67 staining along the dermal-epidermal border indicates proliferation of epidermal basal stem cells and, consistent with inflammation, staining of lymphocytes highlights the increased proliferation of infiltrating T cells.

Supplementary Figure 8.

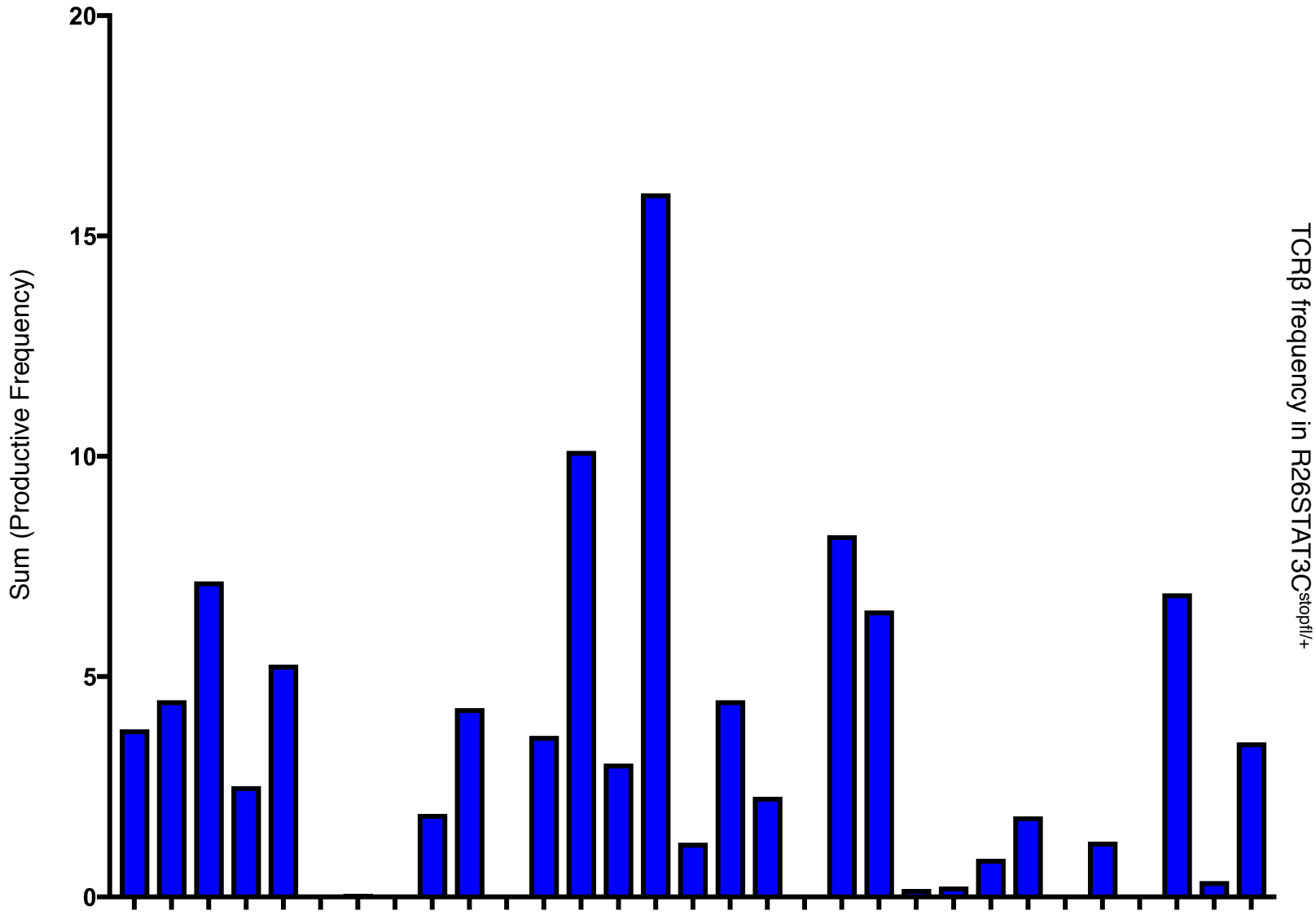

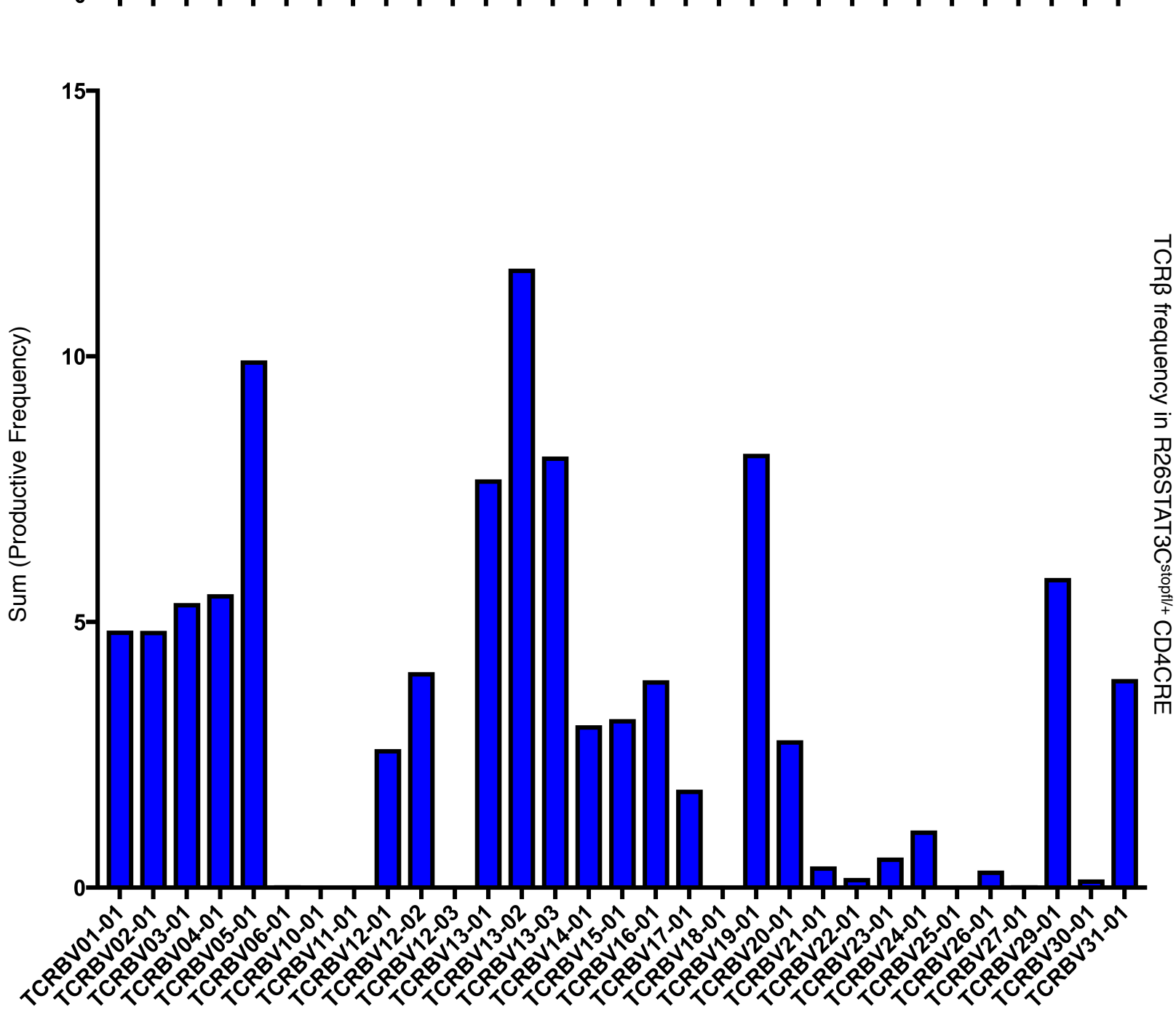

Figure S8. TCRβ frequency in the skin of *R26STAT3C$^{stopfl/+}$ CD4Cre* and control mice.
The frequency of V beta gene usage for T cells from the skin of *R26STAT3C$^{stopfl/+}$ CD4Cre* and control mice. Mice are between 12-15 months old. Each is representative of three independent samples sequenced.

Supplementary Figure 9.

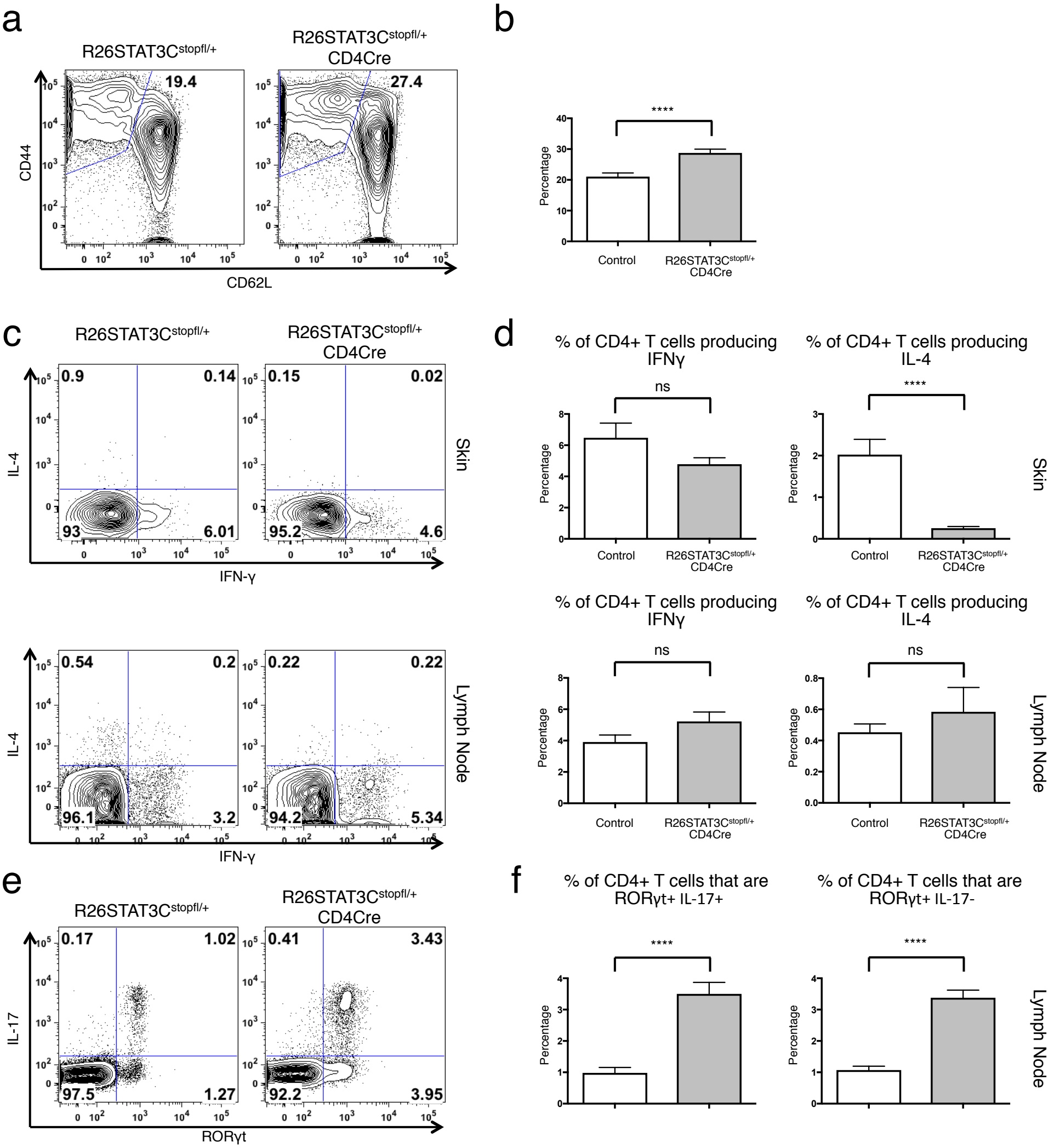

Figure S9. Activation, cytokine production, and RORγt expression in CD4+ T cells of the skin and lymph nodes of *R26STAT3C$^{stopfl/+}$ CD4Cre* and control mice.

(a) Representative flow cytometry analysis of activated (CD44^{hi}, CD62L^{lo}) CD3+CD4+ T cells from peripheral lymph nodes of 11.5 month old *R26STAT3C$^{stopfl/+}$ CD4Cre* and control mice. (b) Quantification of the percentage of activated (CD44^{hi}, CD62L^{lo}) CD3+CD4+ cells isolated from the peripheral lymph nodes of *R26STAT3C$^{stopfl/+}$ CD4Cre* and control mice. Data is from 11 independent experiments n≥13 for each genotype. Mice range from 7-13 months old (c) Representative flow cytometry analysis of CD3+CD4+ T cells from the skin and peripheral lymph nodes of 8.5-11 month old *R26STAT3C$^{stopfl/+}$ CD4Cre* and control mice stained for IL-4 and IFNγ (d) Top: Quantification of cytokine production from CD3+CD4+ T cells isolated from skin. Data is from ≥16 independent experiments. n≥17 for each genotype, ages 6-16 months old. Bottom: Quantification of cytokine expression from CD3+CD4+ T cells isolated from peripheral lymph nodes. Data is from 21 independent experiments. n≥25 for each genotype, ages 6-16 months old. E) Representative intracellular flow cytometry analysis of IL-17 production in RORγt+ CD3+CD4+ T cells isolated from the peripheral lymph nodes of R26STAT3C$^{stopfl/+}$ CD4Cre and control mice, ages 11 months old. (f) Left: Quantification of the percentage of RORγt+ IL-17+cells. Right: Quantification of the percentage of RORγt+ IL-17- cells. Cells were gated on CD3+CD4+ T cells isolated from peripheral lymph nodes, n=9 for each genotype, ages 10-13. For all flow data statistical significance was assessed using the nonparametric two-tailed Mann-Whitney U test. Significance values are as follows: ns ($p > 0.05$), * ($p \leq 0.05$), ** ($p \leq 0.01$), *** ($p \leq 0.001$) **** ($p \leq 0.0001$). Values shown as mean ± SEM.

Supplementary Table 1.

Top 124 differentially expressed genes between Sézary Syndrome Cells and Memory T Cells

HDAC9	PTMS	RP11-105N14.1	AC079610.1
TNFSF11	RHOB	KLHL42	TRIP10
IL17REL	C1orf105	MAGI1	TTBK1
RP11-664H17.1	GNG4	RPS20P22	BACH1-IT3
CD70	TFAP2A	MIR199A2	TMEM38A
RP11-405A12.2	MLF1	NKX6-3	RPL7P50
DNM3	KSR2	KCNN4	ZNF860
NEDD4L	DNAH14	KRT18P37	PTH2R
C16orf45	CLEC4M	FZD1	C3orf14
CSF2RB	HPGDS	FAM174B	ZNF334
TPO	SGCE	BCAS1	PCDHGB1
KIAA1199	CPA5	IRAK3	FSCN1
TNFSF9	MYB	AC006129.4	PHEX
TBX20	HCAR1	CD9	PGM2L1
TWIST1	RP11-121L10.3	RP11-78H18.2	HRH1
RP11-845C23.2	NDUFA4L2	RP11-521B24.3	ITM2C
DISC1FP1	GRAMD1C	MRC2	RP11-593F23.1
POF1B	KCNK1	CPNE2	HOTAIRM1
RP11-281P23.1	GALNT9	SPERT	RN7SKP184
MIR214	KIF26B	LMNA	ARAP3
ENOX1	RDH10	MIOX	EVC
AIRE	FGFR1	PLEKHH3	IGFBP4
FLNC	PCDHGA10	GRIN3A	SH2D6
AP000351.10	PTPLA	RFTN2	HOMER2
KRT1	CES3	IGSF9B	PIM3
OSBPL10	ALG1L	FAAH	TSHZ2
ANK1	PTHLH	CDO1	DUSP4
ZNF233	RAPH1	IKZF2	MFSD10
RP11-407A16.3	SSC5D	RP11-405A12.1	KALRN
KB-226F1.1	RP11-993B23.3	CACNA1H	LAYN
PDE7B	HTATSF1P2	NRP1	GPR55

Supplemental Table 1. Gene signature for Sézary Syndrome Cells
A list of the top 124 differentially expressed genes between SS cells and Memory T Cells from healthy patients. The gene were selected based on a difference of expression of 4x or more between SS and Tmem cells and on q value ≤ 0.05